Modelling and index analysis of a Delta-type mechanism

Article *in* Proceedings of the Institution of Mechanical Engineers Part K Journal of Multi-body Dynamics · September 2004

DOI: 10.1243/1464419042035944

CITATIONS
12

READS
180

4 authors, including:

Mansour Karkoub
Texas A&M University
129 PUBLICATIONS **1,155** CITATIONS
SEE PROFILE

Ming-Cheng Tsai
National Taiwan University
128 PUBLICATIONS **2,745** CITATIONS
SEE PROFILE

Ming-Guo Her
Tatung University
62 PUBLICATIONS **536** CITATIONS
SEE PROFILE

Modelling and index analysis of a Delta-type mechanism

K-S Hsu[1*], **M Karkoub**[2], **M-C Tsai**[3] and **M-G Her**[4]
[1]Department of Automation Engineering, Kao Yuan Institute of Technology, Lu-Chu Hsiang, Kaohsiung, Taiwan, China
[2]Department of Mechanical and Industrial Engineering, College of Engineering and Petroleum, Kuwait University, Kuwait
[3]Department of Mechanical Engineering, National Cheng Kung University, Tainan, Taiwan
[4]Department of Mechanical Engineering, Tatung University, Taipei, Taiwan

Abstract: A new type of three-dimensional parallel robot with a human interface as well as parallel motion control of a platform manipulator actuated by three a.c. servomotors is presented in this paper. The performance of this parallel robot is analysed using its forward and inverse kinematics. The analysis is performed using known quantified and graphical performance synthesis tools. Computer simulations of the parallel robot system have shown good correlation between physical interpretations and the results of using the theoretical analysis tools.

Keywords: three-dimensional parallel robot arm, graphical performance, workspace, path configuration

NOTATION

a	length of link $\overline{A_iB_i}$
A_i–$x_iy_iz_i$	reference coordinate of the ith limb
b	length of link $\overline{B_iC_i}$
h	length of link $\overline{PC_i}$
$\mathbf{J}$	Jacobian matrix
$\mathbf{J}_g$	generalized Jacobian
$(\mathbf{J})_{x-y}$	matrix taken out from the Jacobian matrix with first and second rows
$(\mathbf{J}_g)_{x-y}$	generalized Jacobian of $(\mathbf{J})_{x-y}$
LEI	local efficiency index
LKCI	local kinematic cross-coupling index
LMI	local mobility index
O–xyz	reference coordinate of the fixed platform
$\boldsymbol{p}$	position vector of the centroid of the moving platform
r	length of link $\overline{OA_i}$
T_1, T_2	column vectors of the Jacobian matrix
$\boldsymbol{v}_p$	linear velocity of the moving platform
β_{12}	angle of intersection between T_1 and T_2
θ_{1i}	angle measured from the x_i axis to $\overline{A_iB_i}$
θ_{2i}	angle defined from the extended line of $\overline{A_iB_i}$ to the line defined by the intersection of the plane of the parallelogram and the x_i–z_i plane
θ_{3i}	angle measured from the y_i axis to $\overline{B_iC_i}$
$\lambda_{\max,\mathbf{J}_g}$	maximum eigenvalue of $\mathbf{J}_g$
$\lambda_{\min,\mathbf{J}_g}$	maximum eigenvalue of $\mathbf{J}_g$
ϕ_i	angle measured from the x axis to the x_i axis
$\boldsymbol{\omega}_{ji}$	linear velocity of the jth link of the ith limb

1 INTRODUCTION

It is well known that industrial robots play an important role in the automation industry. The speed and accuracy of robotic systems, classified in two typical groups (serial and parallel), are a major concern for many researchers. In the case of serial robots, the displacement of the end-effector is obtained by a serialization of modules, resulting in a large workspace. Moreover, the accuracy of these serial robots is affected by cumulative errors of all the limbs. Another problem with serial robots is the fact that the actuators are mounted on the limbs themselves, resulting in an increase in the total weight of these robots and thus changing some of the characteristics of the systems such as power requirement and natural frequencies. However, in the case of parallel robots, the displacement of the moving plate is a result of the movement of some or all of the articulated limbs mounted on the base, resulting in a smaller workspace than in the case of serial-type robots. However, in spite of the fact that parallel robots have many

Q1 *The MS was received on 25 December 2003 and was accepted after revision for publication on 2 June 2004.*

**Corresponding author: Department of Automation Engineering, Kao Yuan Institute of Technology, 1821 Chung-Shan Road, Lu-Chu Hsiang, Kaohsiung, Taiwan 821, China.*

advantages, they also have some drawbacks that need to be taken into consideration in the design process. For example, since the moving mass in parallel robots is smaller than in the case of serial ones, the natural frequencies of these systems tend to be higher than those of serial robots. Moreover, the total torque output of parallel robots is usually smaller than those of the serial type. However, it is worth noting that, in spite of these disadvantages, parallel robots are preferred in many instances, which explains the increasing interest in the design and control of such manipulators.

Many researchers have focused on the synthesis and analysis of parallel mechanisms for more than two decades. Many types of parallel robot have been created, the most classic of which is the Stewart platform [**1**, **2**]. Another type of parallel mechanism is the Delta Robot which was synthesized in reference [**3**]. Some researchers have dwelt upon the kinematic aspect of this type of mechanism [**4**–**7**], others on the workspace [**8**]. In the present paper a parallel-type robot is synthesized and analysed. The forward and inverse kinematics are derived here to be used for performance analysis. Some performance indices are defined and used to characterize the behaviour of the system as well as to predict the workspace of the system. These indices are based on analysis and graphical interpretation of the Jacobian matrix.

The rest of the paper is organized as follows: a description of the Delta robot is given in section 2. The inverse and forward kinematics as well as the Jacobian of the parallel robot are derived in section 3. Some performance analysis tools are presented in section 4. The results of the performance analysis are presented in section 5. Finally, some concluding remarks are given in section 6.

2 DESCRIPTION OF THE PARALLEL ROBOT

The parallel robot shown in Fig. 1 is a Delta-type robot, which consists of four different parts: the moving platform, the follower rods, the actuated arms and the base. Each actuated arm is connected to two follower rods via three-degree-of-freedom joints. The joints are a combination of a universal joint and a bearing. The follower rods are themselves connected to the moving platform through the same type of three-degree-of-freedom joints, i.e. a combination of a universal joint and a bearing. The total number of degrees of freedom of the Delta mechanism can be calculated using Gruebler's equation

$$M = 6(n-1) - 5f_1 - 4f_2 - 3f_3 \tag{1}$$

where M is the number of degrees of freedom in the mechanism, n is the number of links, f_1 is the number of single-degree-of-freedom joints, f_2 is the number of two-degree-of-freedom joints and f_3 is the number of three-degree-of-freedom joints. For this particular mechanism, $n = 11$, $f_1 = 3$, $f_2 = 0$ and $f_3 = 12$. Substituting these numbers into (1) leads to $M = 9$. It is worth noting that

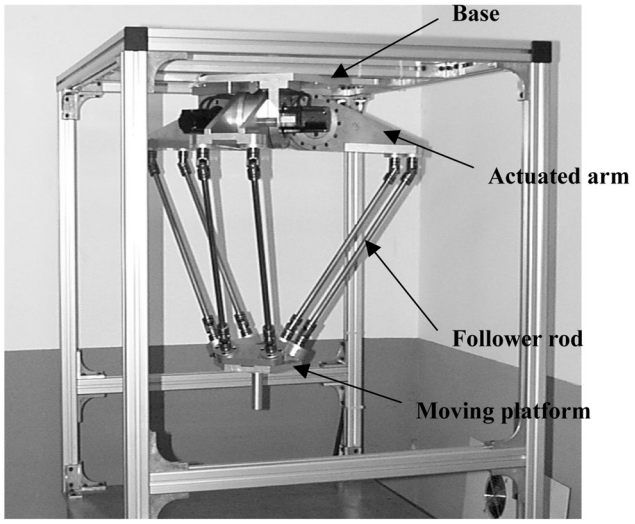

Fig. 1 Delta-type robot

Gruebler's equation presented in this paper accounts for all degrees of freedom including internal (or parasitic) ones. Parasitic degrees of freedom of internal bodies do not usually affect the motion of the platform but definitely increase the geometric complexity of the model. Therefore, since six of these degrees of freedom of the mechanism correspond to the rotation of the follower rods (internal), the moving platform actually has three degrees of freedom only (x, y, and z directions) [**9**].

3 KINEMATIC ANALYSIS

For robot position control and path configuration, it is necessary to obtain the inverse and forward kinematics of the robot [**10**]. The inverse kinematics is first derived here, followed by the forward kinematics.

3.1 Inverse kinematics

As shown in Fig. 2, a reference coordinate system O–xyz is attached to the centre O of the fixed platform where the x and y axes lie on the fixed plane and the z axis points upwards vertically. Another coordinate system A_i–$x_iy_iz_i$ is attached to the fixed base at point A_i, such that the x_i axis is in line with the extended line $\overline{OA_i}$, the y_i axis is directed along the revolute joint axis at A_i and the z_i axis is parallel to the z axis. The angle ϕ_i is measured from the x axis to the x_i axis, and it is a constant parameter of the manipulator design. Figure 3 defines the joint angles associated with the ith limb, where $\boldsymbol{p}$ is the position vector of the centroid of the moving platform, θ_{1i} is measured from the x_i axis to $\overline{A_iB_i}$, θ_{2i} is defined from the extended line of $\overline{A_iB_i}$ to the line defined by the intersection of the plane of the parallelogram and the x_i–z_i plane and θ_{3i} is measured from the y_i direction to $\overline{B_iC_i}$. Overall, there are nine joint angles, θ_{1i}, θ_{2i}, and θ_{3i} for $i = 1$, 2 and 3, associated with the manipulator. The actuated joint angles are θ_{11}, θ_{12}, and θ_{13}.

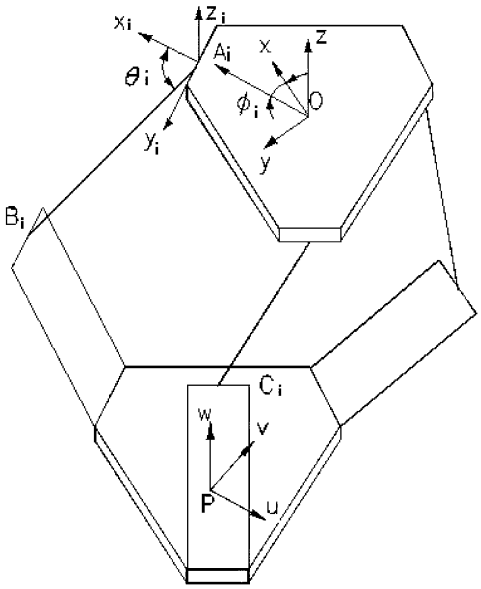

Fig. 2 Sketch map of the Delta-type robot

Q2 A loop-closure equation can be written for each limb

$$\boldsymbol{A_iB_i} + \boldsymbol{B_iC_i} = \boldsymbol{OP} + \boldsymbol{PC_i} - \boldsymbol{OA_i} \tag{2}$$

Rewriting (2) in the A_i–$x_iy_iz_i$ coordinate frame leads to

$$\begin{bmatrix} a\cos\theta_{1i} + b\sin\theta_{3i}\cos(\theta_{1i}+\theta_{2i}) \\ b\cos\theta_{3i} \\ a\sin\theta_{1i} + b\sin\theta_{3i}\sin(\theta_{1i}+\theta_{2i}) \end{bmatrix} = \begin{bmatrix} c_{xi} \\ c_{yi} \\ c_{zi} \end{bmatrix} \tag{3}$$

where

$$\begin{bmatrix} c_{xi} \\ c_{yi} \\ c_{zi} \end{bmatrix} = \begin{bmatrix} \cos\phi_i & \sin\phi_i & 0 \\ -\sin\phi_i & \cos\phi_i & 0 \\ 0 & 0 & 1 \end{bmatrix} \begin{bmatrix} p_x \\ p_y \\ p_z \end{bmatrix} + \begin{bmatrix} h-r \\ 0 \\ 0 \end{bmatrix} \tag{4}$$

denotes the position of C_i relative to the A_i–$x_iy_iz_i$ coordinate frame, a and b are the lengths of links $\overline{A_iB_i}$ and $\overline{B_iC_i}$ respectively and $\boldsymbol{p} = [p_x\, p_y\, p_z]^{\mathrm{T}}$ is the position vector of point P relative to the O–xyz coordinate system.

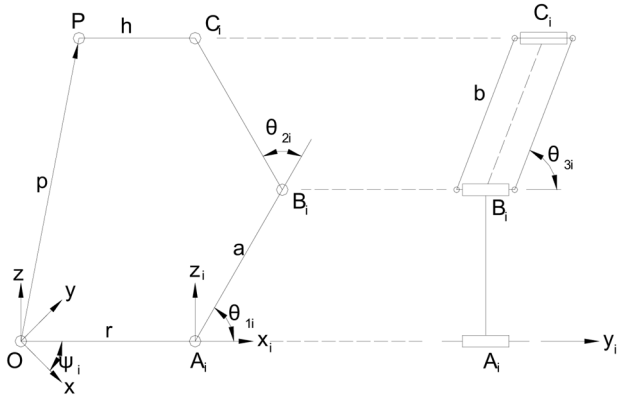

Fig. 3 Description of the joint angles

The angle θ_{3i} is found by solving the second row of equation (3)

$$\theta_{3i} = \cos^{-1}\frac{c_{yi}}{b} \tag{5}$$

With θ_{3i} determined, an equation with θ_{2i} as the only unknown is generated by summing the squares of c_{xi},c_{yi} and c_{zi} in equation (3)

$$2ab\sin\theta_{3i}\cos\theta_{2i} + a^2 + b^2 = c_{xi}^2 + c_{yi}^2 + c_{zi}^2 \tag{6}$$

Hence

$$\theta_{2i} = \cos^{-1}\kappa \tag{7}$$

where

$$\kappa = \frac{c_{xi}^2 + c_{yi}^2 + c_{zi}^2 - a^2 - b^2}{2ab\sin\theta_{3i}}$$

With θ_{3i} and θ_{2i} determined, a pair of equations with θ_{1i} as the only unknown is derived using equation (3). Therefore, it is possible to solve for θ_{1i} numerically.

3.2 Forward kinematics

To obtain the forward kinematics of the parallel mechanism, the following is done. Substituting c_{xi},c_{yi}, and c_{zi} from equation (4) into equation (3) yields

$$\begin{bmatrix} b\sin\theta_{3i}\cos(\theta_{1i}+\theta_{2i}) \\ b\cos\theta_{3i} \\ b\sin\theta_{3i}\sin(\theta_{1i}+\theta_{2i}) \end{bmatrix} = \begin{bmatrix} \cos\phi_i & \sin\phi_i & 0 \\ -\sin\phi_i & \cos\phi_i & 0 \\ 0 & 0 & 1 \end{bmatrix} \times \begin{bmatrix} p_x \\ p_y \\ p_z \end{bmatrix} + \begin{bmatrix} -a\cos\theta_{1i} - r + h \\ 0 \\ -a\sin\theta_{1i} \end{bmatrix} \tag{8}$$

An equation is obtained by summing the squares of the three components of equation (8)

$$\begin{aligned} b^2 = {} & p_x^2 + p_y^2 + p_z^2 - 2(p_x\cos\phi_i + p_y\sin\phi_i) \\ & \times (a\cos\theta_{1i} + r - h) - 2p_z a\sin\theta_i \\ & + (a\cos\theta_i + r - h)^2 + a^2\sin^2\theta_i \quad (\text{for } i = 1,\ 2,\ 3) \end{aligned} \tag{9}$$

Subtracting equation (9) at $i = 1$ from equation (9) at $i = j$ leads to

$$e_{1j}p_x + e_{2j}p_y + e_{3j}p_z + e_{4j} = 0 \qquad (\text{for } j = 2 \text{ and } 3) \tag{10}$$

where

$$
\begin{aligned}
e_{1j} &= 2\cos\phi_j(a\cos\theta_{1j} + r - h) \\
&\quad - 2\cos\phi_1(a\cos\theta_{11} + r - h) \\
e_{2j} &= 2\sin\phi_j(a\cos\theta_{1j} + r - h) \\
&\quad - 2\sin\phi_1(a\cos\theta_{11} + r - h) \\
e_{3j} &= 2a\sin\theta_{1j} - 2a\sin\theta_{11} \\
e_{4j} &= (a\cos\theta_{1j} + r - h)^2 - a^2\sin^2\theta_{1j} \\
&\quad - (a\cos\theta_{11} + r - h)^2 - a^2\sin^2\theta_{11}
\end{aligned}
$$

Expansion of equation (10) for $j = 2$ and 3 results in two linearly independent equations.

Solving equation (10) for p_x and p_z in terms of p_y and then substituting into equation (9) for $i = 1$ yields

$$k_0 p_x^2 + k_1 p_x + k_2 = 0 \tag{11}$$

The coefficients of the quadratic equation (11) are given by

$$
\begin{aligned}
k_0 &= 1 + \frac{l_1^2}{l_2^2} + \frac{l_4^2}{l_2^2} \\
k_1 &= \frac{2l_0 l_1}{l_2^2} + \frac{2l_3 l_4}{l_2^2} - 2l_5\cos\phi_1 - \frac{2l_5 l_1}{l_2}\sin\phi_1 \\
&\quad - \frac{2al_4}{l_2}\sin\theta_{11} \\
k_2 &= l_5^2 - b^2 + \frac{l_0^2}{l_2^2} + \frac{l_3^2}{l_2^2} + a^2\sin^2\theta_{11} - \frac{2l_5 l_1}{l_2}\sin\phi_1 \\
&\quad - \frac{2al_3}{l_2}\sin\theta_{11}
\end{aligned}
$$

where

$$
\begin{aligned}
l_0 &= e_{32}e_{43} - e_{33}e_{42} \\
l_1 &= e_{13}e_{32} - e_{12}e_{33} \\
l_2 &= e_{22}e_{33} - e_{23}e_{32} \\
l_3 &= e_{23}e_{42} - e_{22}e_{43} \\
l_4 &= e_{12}e_{23} - e_{13}e_{22} \\
l_5 &= ac\theta_{11} + r - h
\end{aligned}
$$

Once p_x is found, the values for p_y and p_z are obtained by back substitution into equation (10).

3.3 Singularity analysis

Q3 Referring to Fig. 3, a loop-closure equation for the ith limb can be written as

$$\boldsymbol{OP} + \boldsymbol{PC}_i = \boldsymbol{OA}_i + \boldsymbol{A}_i\boldsymbol{B}_i + \boldsymbol{B}_i\boldsymbol{C}_i \tag{12}$$

Differentiating equation (12) with respect to time yields

$$\boldsymbol{v}_p = \boldsymbol{\omega}_{1i} \times \boldsymbol{a}_i + \boldsymbol{\omega}_{2i} \times \boldsymbol{b}_i \tag{13}$$

where $\boldsymbol{v}_p = [v_{\mathrm{p},x}\ v_{\mathrm{p},y}\ v_{\mathrm{p},z}]^{\mathrm{T}}$ is the linear velocity of the moving platform, $\boldsymbol{a}_i = \overline{A_iB_i}$, $\boldsymbol{b}_i = \overline{B_iC_i}$ and $\boldsymbol{\omega}_{ji}$ is the angular velocity of the jth link of the ith limb. To eliminate $\boldsymbol{\omega}_{2i}$, it is necessary to dot-multiply both sides of equation (13) and $\boldsymbol{b}_i$. Therefore

$$\boldsymbol{b}_i \cdot \boldsymbol{v}_{\mathrm{p}} = \boldsymbol{\omega}_{1i} \cdot (\boldsymbol{a}_i \times \boldsymbol{b}_i) \tag{14}$$

Rewriting the vectors of equation (14) in the A_i–$x_iy_iz_i$ coordinate frame leads to

$$
\boldsymbol{a}_i = a\begin{bmatrix}\cos\theta_{1i}\\ 0\\ \sin\theta_{1i}\end{bmatrix}, \qquad \boldsymbol{b}_i = b\begin{bmatrix}\sin\theta_{3i}\cos(\theta_{1i}+\theta_{2i})\\ \cos\theta_{3i}\\ \sin\theta_{3i}\sin(\theta_{1i}+\theta_{2i})\end{bmatrix}
$$

$$
\boldsymbol{\omega}_i = \begin{bmatrix}0\\ -\dot{\theta}_{1i}\\ 0\end{bmatrix} \qquad \boldsymbol{v}_{\mathrm{p}} = \begin{bmatrix}v_{\mathrm{p},x}\cos\phi_i + v_{\mathrm{p},y}\sin\phi_i\\ -v_{\mathrm{p},x}\sin\phi_i + v_{\mathrm{p},y}\cos\phi_i\\ v_{\mathrm{p},z_i}\end{bmatrix}
$$

Substituting the values of $\boldsymbol{a}_i, \boldsymbol{b}_i, \boldsymbol{\omega}_i$ and $\boldsymbol{v}_{\mathrm{p}}$ in equation (14) leads to

$$j_{ix}v_{\mathrm{p},x} + j_{iy}v_{\mathrm{p},y} + j_{iz}v_{\mathrm{p},z} = a\sin\theta_{2i}\sin\theta_{3i}\dot{\theta}_{1i} \tag{15}$$

where

$$
\begin{aligned}
j_{ix} &= \cos(\theta_{1i}+\theta_{2i})\sin\theta_{3i}\cos\phi_i - \cos\theta_{3i}\sin\phi_i \\
j_{iy} &= \cos(\theta_{1i}+\theta_{2i})\sin\theta_{3i}\sin\phi_i + \cos\theta_{3i}\cos\phi_i \\
j_{iz} &= \sin(\theta_{1i}+\theta_{2i})\sin\theta_{3i}
\end{aligned} \tag{16}
$$

Expanding equation (15) for $i = 1, 2$ and 3 yields three scalar equations which can be assembled into a matrix form as

$$\mathbf{J}_x\boldsymbol{v}_{\mathrm{p}} = \mathbf{J}_q\dot{\boldsymbol{q}} \tag{17}$$

where

$$
\mathbf{J}_x = \begin{bmatrix} j_{1x} & j_{1y} & j_{1z} \\ j_{2x} & j_{2y} & j_{2z} \\ j_{3x} & j_{3y} & j_{3z} \end{bmatrix} \tag{18}
$$

$$
\mathbf{J}_q = a\begin{bmatrix} \sin\theta_{21}\sin\theta_{31} & 0 & 0 \\ 0 & \sin\theta_{22}\sin\theta_{32} & 0 \\ 0 & 0 & \sin\theta_{23}\sin\theta_{33} \end{bmatrix} \tag{19}
$$

$$\dot{\boldsymbol{q}} = [\dot{\theta}_{11}\ \dot{\theta}_{12}\ \dot{\theta}_{31}]^{\mathrm{T}}$$

After algebraic manipulations, it is possible to write

$$\boldsymbol{v}_{\mathrm{p}} = \mathbf{J}\dot{\boldsymbol{q}} \tag{20}$$

where

$$\mathbf{J} = \mathbf{J}_x^{-1}\mathbf{J}_q \equiv \begin{bmatrix} \dfrac{\partial x}{\partial \theta_1} & \dfrac{\partial x}{\partial \theta_2} & \dfrac{\partial x}{\partial \theta_3} \\ \dfrac{\partial y}{\partial \theta_1} & \dfrac{\partial y}{\partial \theta_2} & \dfrac{\partial y}{\partial \theta_3} \\ \dfrac{\partial z}{\partial \theta_1} & \dfrac{\partial z}{\partial \theta_2} & \dfrac{\partial z}{\partial \theta_3} \end{bmatrix}$$

From equation (17) it can be observed that singularity occurs:

1. when $\det(\mathbf{J}_q) = 0$. This means that either $\theta_{2i} = 0$ or π, or $\theta_{3i} = 0$ or π, for $i = 1$, 2 or 3.
2. when $\det(\mathbf{J}_x) = 0$. This means that $\theta_{1i} + \theta_{2i} = 0$ or π, or $\theta_{3i} = 0$ or π, for $i = 1$, 2 and 3. In addition, singularities occur when $j_i = \pm j_k$ in matrix $\mathbf{J}_x$ for $i \neq k$.
3. when $\det(\mathbf{J}_q) = 0$ and $\det(\mathbf{J}_q) = 0$. This situation occurs when $\theta_{3i} = 0$ or π for $i = 1$, 2 and 3.

In summary, singularity of the parallel manipulator occurs:

1. When all three pairs of the follower rods are parallel. Therefore, the moving platform has three degrees of freedom and moves along a spherical surface and rotates about the axis perpendicular to the moving platform (see Fig. 4).
2. When two pairs of the follower rods are parallel. The moving platform has one degree of freedom; i.e. the moving platform moves in one direction only (see Fig. 5).
3. When two pairs of the follower rods are in the same plane or two parallel planes. The moving platform has one degree of freedom; i.e. the moving platform rotates about the horizontal axis only.

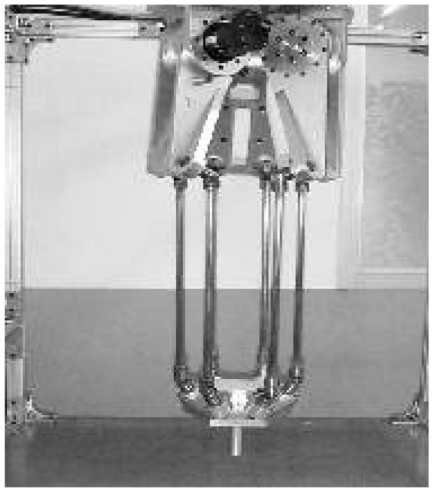

Fig. 4 Singular position when all three pairs of follower rods are parallel to each other

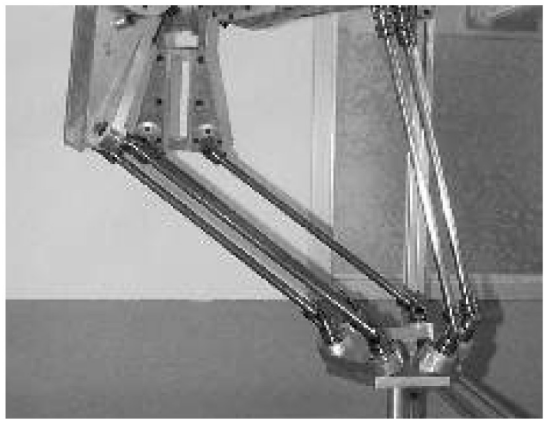

Fig. 5 Singular position when all two pairs of follower rods are parallel to each other

4 PERFORMANCE ANALYSIS

Multi-degree-of-freedom mechanisms such as robotic manipulators have complicated kinematic and kinetic characteristics including cross-coupling among multiple joints, motion degeneration due to singularities and varying velocity/force manipulability depending on the mechanism configuration. With the recent emphasis on quality motion performance, these performance characteristics have become important design factors.

In references [**11**] and [**12**] a tool for representing the kinematic and kinetic performance of mechanisms is proposed. This tool is such that the performance characteristics are quantified analytically and represented graphically. Various performance indices are derived from the Jacobian matrix and its quadratic form. These performance indices are: the local kinematic cross-coupling index (angle of intersection between the column vectors of the Jacobian), the local mobility index (ratio of the Jacobian eigenvalues) and the local efficiency index (product of the Jacobian eigenvalues). The performance characteristics of the mechanism can be represented graphically using eigen-ellipses and workspace trajectory contours.

4.1 Local kinematics cross-coupling index (LKCI)

A serial-type two-link mechanism is used here to illustrate the local kinematics cross-coupling index. The robot mechanism has two degrees of freedom whose joint variables are denoted by θ_1 and θ_2. The class of tasks that has been specified for this mechanism can be described by two variables x and y. Figure 6 shows the trajectory contour diagram. Two contour lines are generated by plotting the location of the end-point of the mechanism in the x–y plane that results from varying one joint variable and keeping the other one

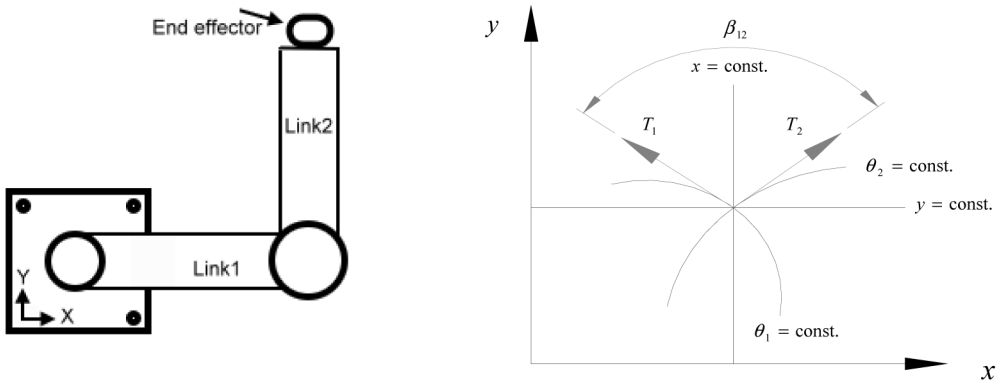

Fig. 6 Trajectory contours of the serial-type two-link mechanism

fixed. Two tangent lines $\boldsymbol{T}_1$ and $\boldsymbol{T}_2$ are obtained at the intersection of the two curves. The tangent lines can be written in matrix form as

$$\boldsymbol{T}_1 = \begin{bmatrix} \dfrac{\partial x}{\partial \theta_1} \\ \dfrac{\partial y}{\partial \theta_1} \end{bmatrix} \quad \text{and} \quad \boldsymbol{T}_2 = \begin{bmatrix} \dfrac{\partial x}{\partial \theta_2} \\ \dfrac{\partial y}{\partial \theta_2} \end{bmatrix} \tag{21}$$

Note that the two tangent vectors correspond to the first two columns of the Jacobian matrix

$$\mathbf{J} \equiv \begin{bmatrix} \dfrac{\partial x}{\partial \theta_1} & \dfrac{\partial x}{\partial \theta_2} \\ \dfrac{\partial y}{\partial \theta_1} & \dfrac{\partial y}{\partial \theta_2} \end{bmatrix} = \begin{bmatrix} \boldsymbol{T}_1 & \boldsymbol{T}_2 \end{bmatrix} \tag{22}$$

The end-point motion of the two-degree-of-freedom mechanism can be generated by a combination of the motion of the joints. If the motion of the joints is highly coupled, this complicates the trajectory generation and motion control. From equation (22), the Jacobian represents the task domain velocity for a unit joint velocity vector. Therefore, the column vector of the Jacobian represents the task domain velocity vector for a given fixed joint velocity. If $\boldsymbol{T}_1$and $\boldsymbol{T}_2$ are linearly dependent, then $\boldsymbol{T}_1$ and $\boldsymbol{T}_2$ become coincident for a given set of joint velocity vectors $\dot{\boldsymbol{\theta}}_1$ and $\dot{\boldsymbol{\theta}}_2$. In contrast, if $\boldsymbol{T}_1$ and $\boldsymbol{T}_2$ are linearly independent, then the two corresponding task domain velocity vectors are orthogonal to each other. In this case, the end-point motion in the directions of these tangent vectors can only be achieved by varying the corresponding joint. Therefore, the cross-coupling between joint motions can be interpreted as a degree of linear dependency between column vectors of the Jacobian matrix. That is, the inner product of the column vectors of the Jacobian provides an indication of joint dependency.

A quantitative measure referred to as the local kinematics cross-coupling index (LKCI) [**11**] for analysing joint dependency is defined as

$$\text{LKCI} \equiv \sin \beta_{12} \tag{23}$$

where β_{12} is the angle of intersection between $\boldsymbol{T}_1$ and $\boldsymbol{T}_2$

$$\beta_{12} = \cos^{-1}\left(\frac{\boldsymbol{T}_1 \boldsymbol{T}_2}{|\boldsymbol{T}_1||\boldsymbol{T}_2|}\right) \tag{24}$$

Note that the LKCI is in the range (0, 1) since β_{12} is in the range (0, π). When LKCI = 1, the column vectors of the Jacobian matrix are linearly independent and the mechanism joint motions are completely decoupled. When LKCI = 0 this corresponds to a singularity position of the mechanism and the motion of the joints is totally coupled. The column vectors of the Jacobian are linearly dependent and the Jacobian [**J**] is rank deficient. For a three-degree-of-freedom mechanism, the Jacobian matrix has three column vectors. Therefore, LKCI is defined as follows

$$\text{LKCI} \equiv \sin \beta_{12} \sin \beta_{23} \sin \beta_{31} \tag{25}$$

where β_{23} is the angle between $\boldsymbol{T}_2$ and $\boldsymbol{T}_3$, and β_{31} is the angle between $\boldsymbol{T}_3$ and $\boldsymbol{T}_1$. Not that LKCI is in the range (0, 1) since β_{12}, β_{23} and β_{31} are all in the range (0, π). When LKCI = 1, this indicates that the follower rods and the actuated arm are decoupled, however, when LKCI = 0, this indicates that the mechanism has reached its singular configuration.

4.2 Local mobility index (LMI)

The generalized Jacobian matrix, $\mathbf{J}_g$, is defined as the quadratic form of the Jacobian matrix

$$\mathbf{J}_g = \mathbf{J}\mathbf{J}^T \tag{26}$$

The eigenvalues of the generalized Jacobian can be considered as the 'system mechanical advantage'. In other

words, the propagation from the input joint torques to the output end-effector force is directly proportional to the eigenvalues of $\mathbf{J}_g$. When the end-point force is in the direction of the maximum eigenvector of $\mathbf{J}_g$, the Euclidean norm of the joint torque vector, $\boldsymbol{\tau}^T\boldsymbol{\tau}$, has a maximum value that is equal to the maximum eigenvalue of $\mathbf{J}_g$, denoted by $\lambda_{\max,\mathbf{J}_g}$. This situation requires the largest joint torque to exert a unit end-point force. Thus, the force manipulability at the end-point of the mechanism is at its worst when a force is exerted in the direction aligned with the maximum eigenvalue of $\mathbf{J}_g$. On the other hand, when the end-point force is in the direction of the minimum eigenvector of $\mathbf{J}_g$, $\tau^T\tau$ has a minimum value that is equal to the minimum eigenvalue of $\mathbf{J}_g$, $\lambda_{\min,\mathbf{J}_g}$. Thus, the local mobility index is defined as

$$\text{LMI} \equiv \frac{\lambda_{\min,\mathbf{J}_g}}{\lambda_{\max,\mathbf{J}_g}} \in [0, 1] \tag{27}$$

The condition where $\mathbf{LMI} = 1$ indicates that the joint torque vector norms are equal to the end-point force exerted in any direction. In this case, all columns of the Jacobian matrix $\mathbf{J}$ are orthogonal, and all columns are of equal magnitude. The condition $\mathbf{LMI} = 0$ implies that the maximum joint torque vector norm approaches infinity, and hence a singularity occurs.

There exists a duality between the velocity and force mobility: when the end-point velocity is in the direction of the maximum eigenvector of $\mathbf{J}_g$, the norm of the joint velocity vector, $\dot{\boldsymbol{\theta}}^T\dot{\boldsymbol{\theta}}$, has a minimum value that is equal to the maximum eigenvalue of $\mathbf{J}_g$, $1/\lambda_{\min,\mathbf{J}_g}$. This indicates that minimum joint velocities are required to generate a unit end-point velocity. Therefore, the motion mobility at the end-point of the mechanism is at its best when the end-point of the mechanism is moving in the direction aligned with the maximum eigenvalue of $\mathbf{J}_g$. On the other hand, when the end-point is moving in the direction of the minimum eigenvector of $\mathbf{J}_g$, $\dot{\boldsymbol{\theta}}^T\dot{\boldsymbol{\theta}}$ has a maximum value equal to the minimum eigenvalue of $\mathbf{J}_g$, $1/\lambda_{\max,\mathbf{J}_g}$. Thus, the best force manipulability points in the workspace are the worst motion mobility points, and vice versa.

These indices can be represented as 'eigen-ellipses'. From Fig. 7 it is known that the ratio squared of the lengths of the major axes of the eigen-ellipses is equal to the value of LMI. Therefore, the shape of the eigen-ellipse gives an indication of the LMI. A thin and narrow eigen-ellipse corresponds to points in the workspace with low LMI. The closer the eigen-ellipse to becoming a circle, the higher is the value of LMI, which means that the mechanism has a higher uniformity. It is worth noting that, at a singular position, the ellipse collapses to a line and the slenderness of the ellipse becomes undefined.

4.3 Local efficiency index (LEI)

The LEI is defined as the product of the eigenvalues of $\mathbf{J}_g$

$$\text{LEI} \equiv \lambda_1\lambda_2\cdots\lambda_m \tag{28}$$

The condition when $\text{LEI} = 0$ indicates that singularity has occurred. In this worst motion efficiency condition, the Euclidean norm of the joint torque vector is equal to zero, the Euclidean norm of the joint velocity vector is equal to infinity and one degree of freedom is lost. On the other hand, when LEI reaches its maximum value, this implies that the mechanism is farthest from any singularity configuration which corresponds to the best operating conditions.

The area of the force eigen-ellipse is equal to $\pi/\sqrt{\lambda_1\lambda_2}$ and the area of the velocity eigen-ellipse is equal to $\pi\sqrt{\lambda_1\lambda_2}$. Referring to Fig. 8, the area of the force eigen-ellipse is not proportional to LEI; however, the area of the velocity eigen-ellipse is. Thus, it is possible to determine LEI from the area of the eigen-ellipse. The smaller the area of the force eigen-ellipse, the bigger is the area of the velocity eigen-ellipse and the higher the value of LEI. In this situation, the mechanism is farthest from its singularity position. On the other hand, the bigger the area of the force eigen-ellipse, the smaller is the area of the velocity eigen-ellipse and the lower the value of LEI. In this situation, the mechanism is nearing a singularity position.

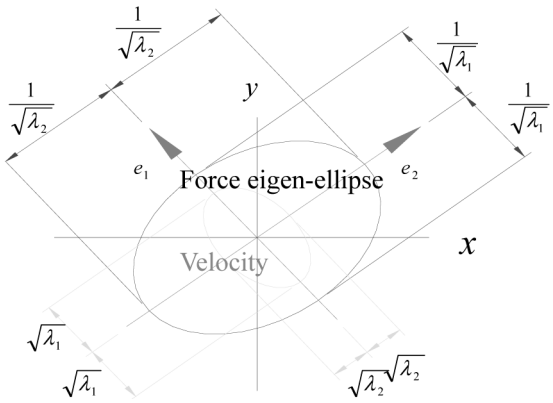

Fig. 7 Force eigen-ellipse and velocity eigen-ellipse

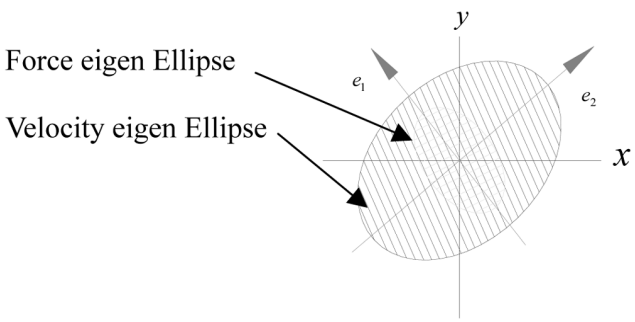

Fig. 8 Area of eigen-ellipse

4.4 Evaluation of performance indices

Substituting equations (16) into equation (18), where $\phi_1 = \pi/3$, $\phi_2 = \pi$ and $\phi_3 = 5\pi/3$, leads to

$$\mathbf{J}_x = \begin{bmatrix} j_{1x} & j_{1y} & j_{1z} \\ j_{2x} & j_{2y} & j_{2z} \\ j_{3x} & j_{3y} & j_{3z} \end{bmatrix}$$

$$= \begin{bmatrix} \frac{1}{2}\cos(\theta_{11}+\theta_{21})\sin\theta_{31} - \frac{\sqrt{3}}{2}\cos\theta_{31} & \frac{\sqrt{3}}{2}\cos(\theta_{11}+\theta_{21})\sin\theta_{31} + \frac{1}{2}\cos\theta_{31} & \sin(\theta_{11}+\theta_{21})\sin\theta_{31} \\ -\cos(\theta_{12}+\theta_{22})\sin\theta_{32} & -\cos\theta_{32} & \sin(\theta_{12}+\theta_{22})\sin\theta_{32} \\ \frac{1}{2}\cos(\theta_{13}+\theta_{23})\sin\theta_{33} + \frac{\sqrt{3}}{2}\cos\theta_{33} & -\frac{\sqrt{3}}{2}\cos(\theta_{13}+\theta_{23})\sin\theta_{33} + \frac{1}{2}\cos\theta_{33} & \sin(\theta_{13}+\theta_{23})\sin\theta_{33} \end{bmatrix}$$

The variable a in equation (19) is equal to 245.42; therefore

$$\mathbf{J}_q = 245.42 \begin{bmatrix} \sin\theta_{21}\sin\theta_{31} & 0 & 0 \\ 0 & \sin\theta_{22}\sin\theta_{32} & 0 \\ 0 & 0 & \sin\theta_{23}\sin\theta_{33} \end{bmatrix}$$

From equation (17), the 3×3 Jacobian matrix is obtained. Since the workspace is the $x-y$ plane, the Jacobian matrix can be reduced to

$$(\mathbf{J})_{x-y} \equiv \begin{bmatrix} \frac{\partial x}{\partial\theta_1} & \frac{\partial x}{\partial\theta_2} & \frac{\partial x}{\partial\theta_3} \\ \frac{\partial y}{\partial\theta_1} & \frac{\partial y}{\partial\theta_2} & \frac{\partial y}{\partial\theta_3} \end{bmatrix}_{2\times3} \tag{29}$$

and the generalized Jacobian can be written as

$$(\mathbf{J}_g)_{x-y} = (\mathbf{J})_{x-y}(\mathbf{J})^{\mathrm{T}}_{x-y} (2\times2 \text{ matrix})$$

Therefore, the eigenvalues and eigenvectors of the generalized Jacobian matrix can be obtained and the performance of the corresponding system can be determined.

5 RESULTS AND DISCUSSION

Figures 9 to 11 show the force eigen-ellipse distribution plots of the $x-y$ planes at $z = 450$, 550 and 650 mm respectively. It is possible to determine the performance characteristics of the system at some point from the shape and size of the eigen-ellipse. The condition when the shape of the eigen-ellipse looks like a circle indicates that the joint torque and velocity vector norms are equal in any direction. On the other hand, the condition when the eigen-ellipse converges to a line implies that the joint torque vector norm approaches infinity in some direction and a degree of freedom is lost: i.e. a singularity occurs. Moreover, the smaller the area of the force eigen-ellipse, the farther is the position from singularity.

The shape of the force eigen-ellipses in the central region looks like a circle, and the size of the force eigen-ellipses is small (see Figs 9 and 11). This indicates that the mechanism has a higher uniformity, and it is far from a singularity position. The shape of the force eigen-ellipses in the region

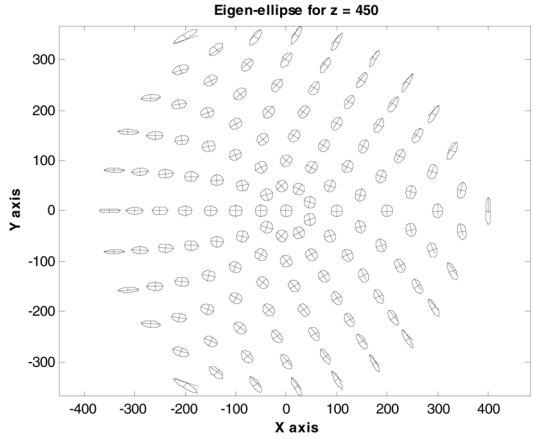

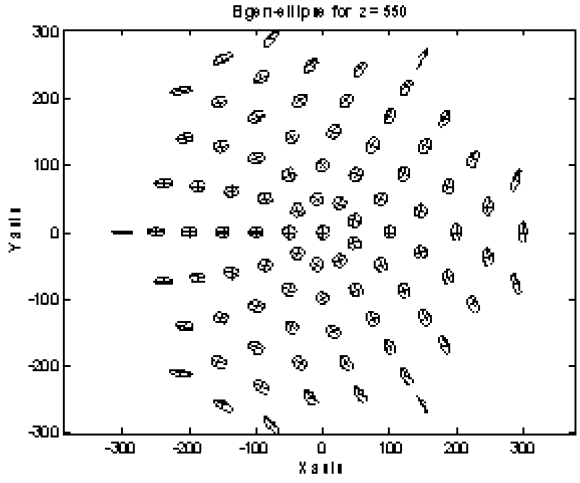

Fig. 10 Force eigen-ellipse and distribution at $z = 550$ mm

Fig. 9 Force eigen-ellipse and distribution at $z = 450$ mm

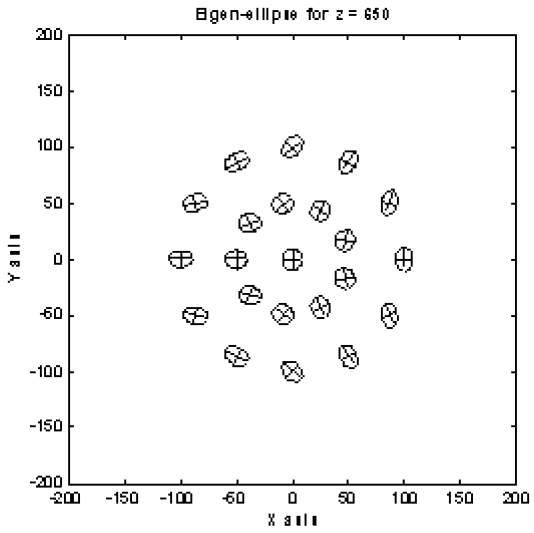

Fig. 11 Force eigen-ellipse and distribution at $z = 650$ mm

away from the centre is thinner and narrower (close to a line). This means that the joint torque vector norm in the direction of the major axis of the force eigen-ellipse approaches infinity, and the mechanism is about to lose a degree of freedom in that direction: i.e. a singularity is about to occur. It is worth noting that the distribution of the force eigen-ellipse is symmetrical about three intersecting axes 120° apart which confirms the positions of the three actuators. From the shape of the distribution of the force eigen-ellipse, the workspace can be found from the positions of the singular points. The workspace is largest when $z = 450$ and smallest when $z = 650$ (see Figs 9 and 11).

Figures 12 to 14 represent the LKCI plots in the x–y planes at $z = 450$, 550 and 650 mm respectively. From the figures it can be seen that the cross-coupling condition occurs at some value of LKCI. The higher the LKCI value, the more linearly independent are the motions of the mechanism joints. On the other hand, the lower the LKCI value, the more coupling there is in the joint motions of the mechanism. The LKCI value in the central region is higher. This indicates that the mechanism has low cross-coupling at that position (see Figs 12 and 14). The LKCI value in the region far from the centre is low, which means that the mechanism exhibits high cross-coupling and is about to lose a degree of freedom in a particular direction: i.e. singularity is about to occur. Again, the distribution of the LKCI plot is symmetrical about three intersecting axes 120° apart which confirms the positions of the three actuators. Moreover, from the distribution of the LKCI value, the workspace can be found from the positions of the singular points: therefore, the workspace and high LKCI region are largest when $z = 450$ and smallest when $z = 650$ (see Figs 12 and 14).

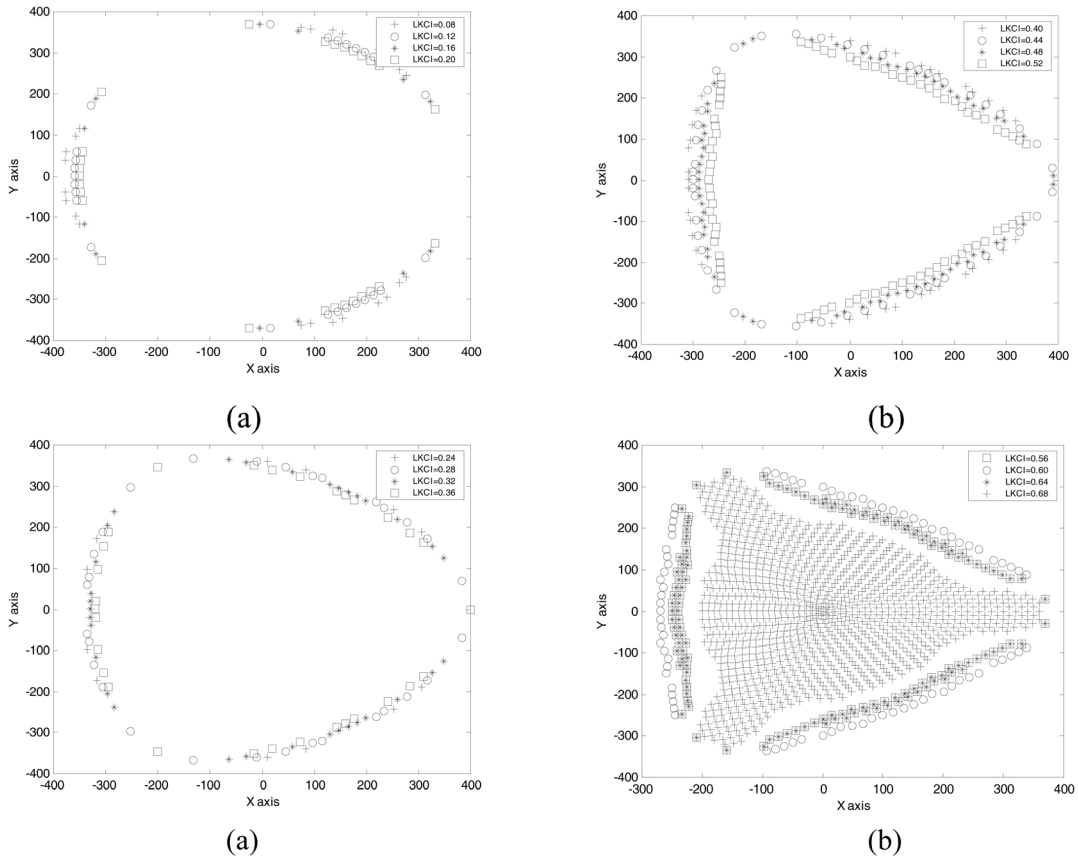

Fig. 12 LKCI plots at $z = 450$ mm

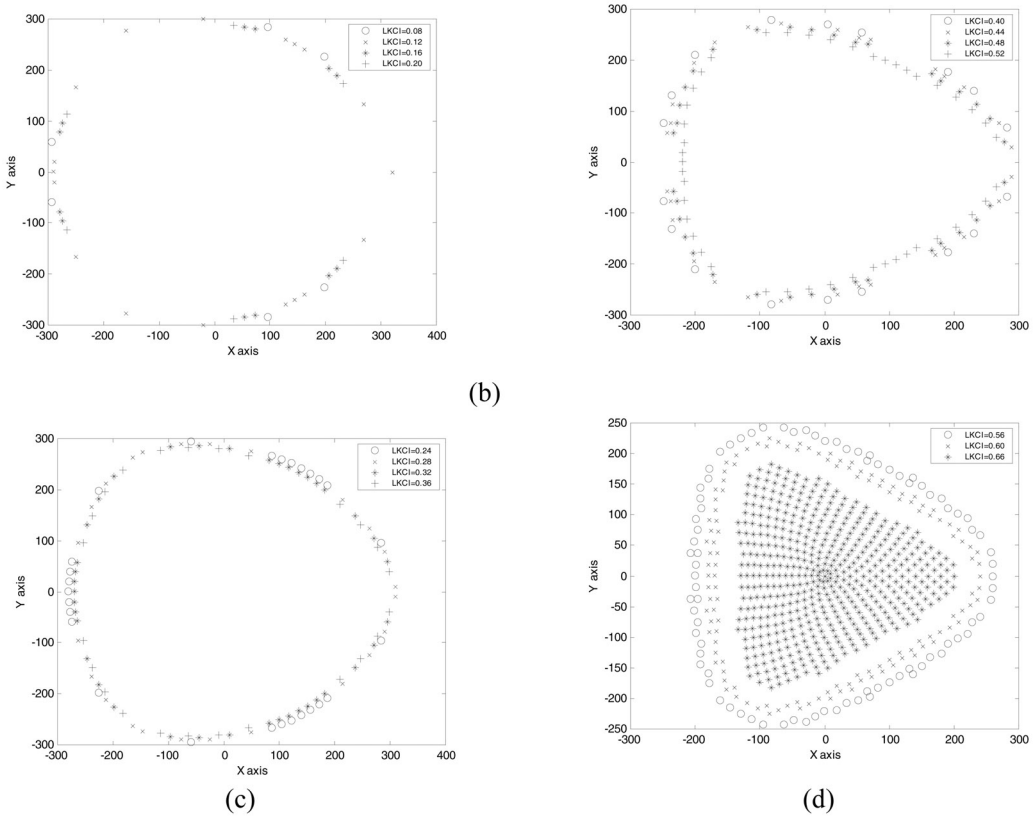

Fig. 13 LKCI plots at $z = 550$ mm

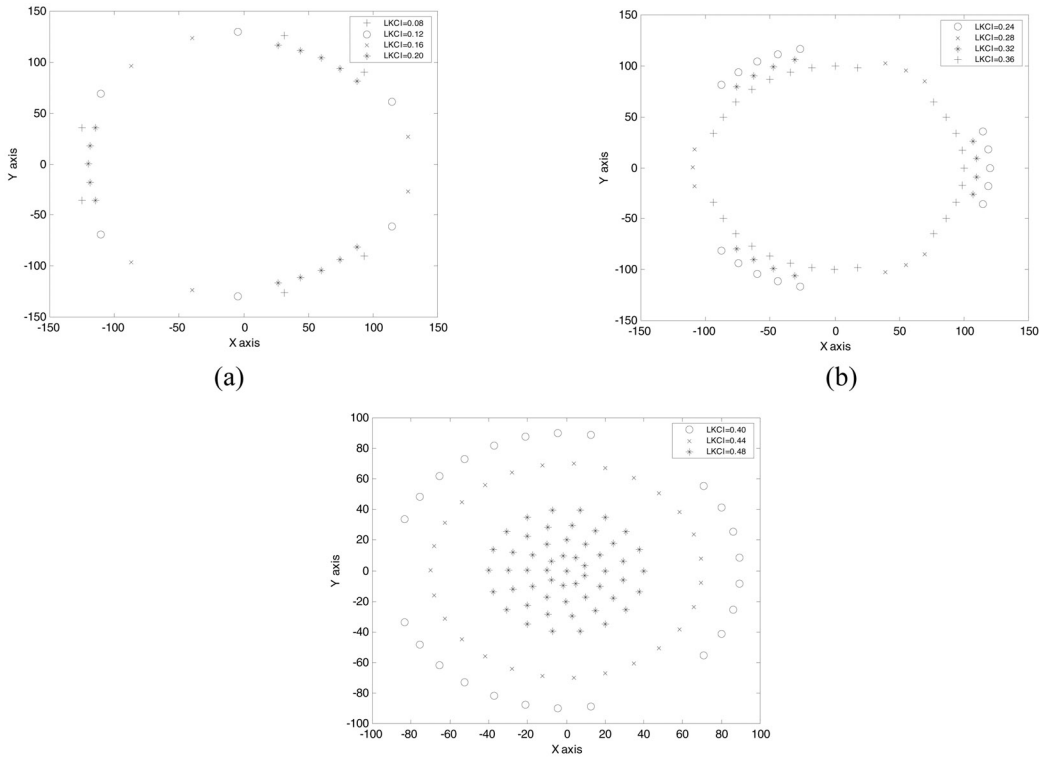

Fig. 14 LKCI plots at $z = 650$ mm

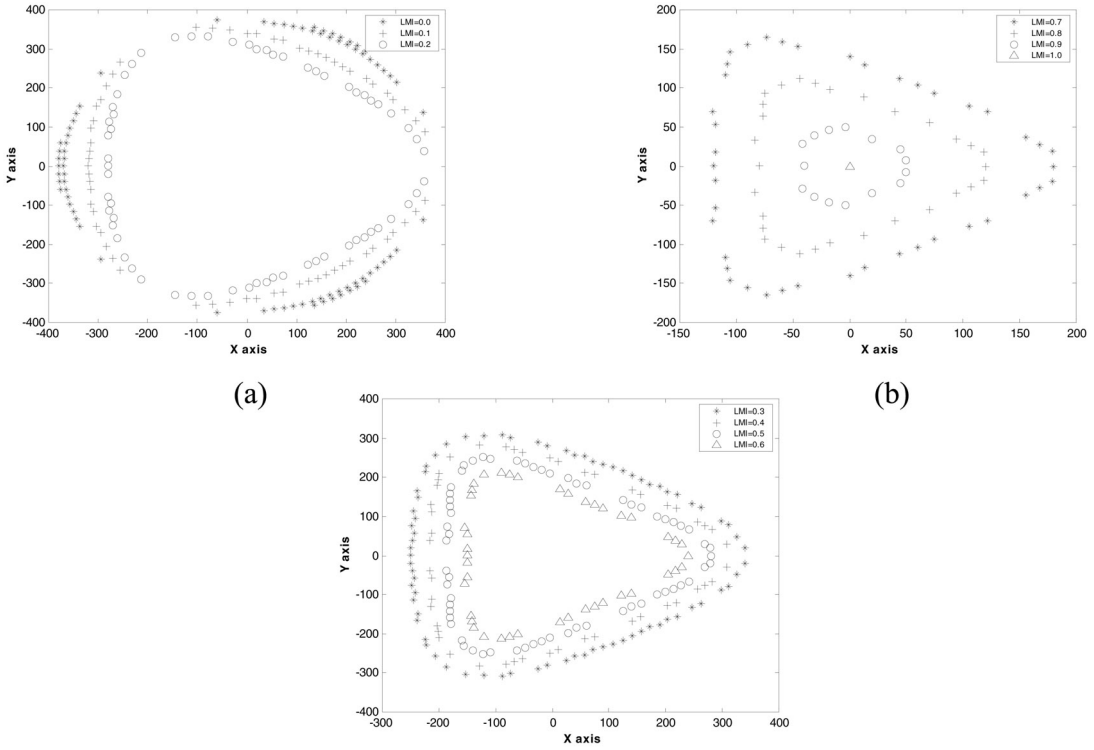

Fig. 15 LMI plots at $z = 450$ mm

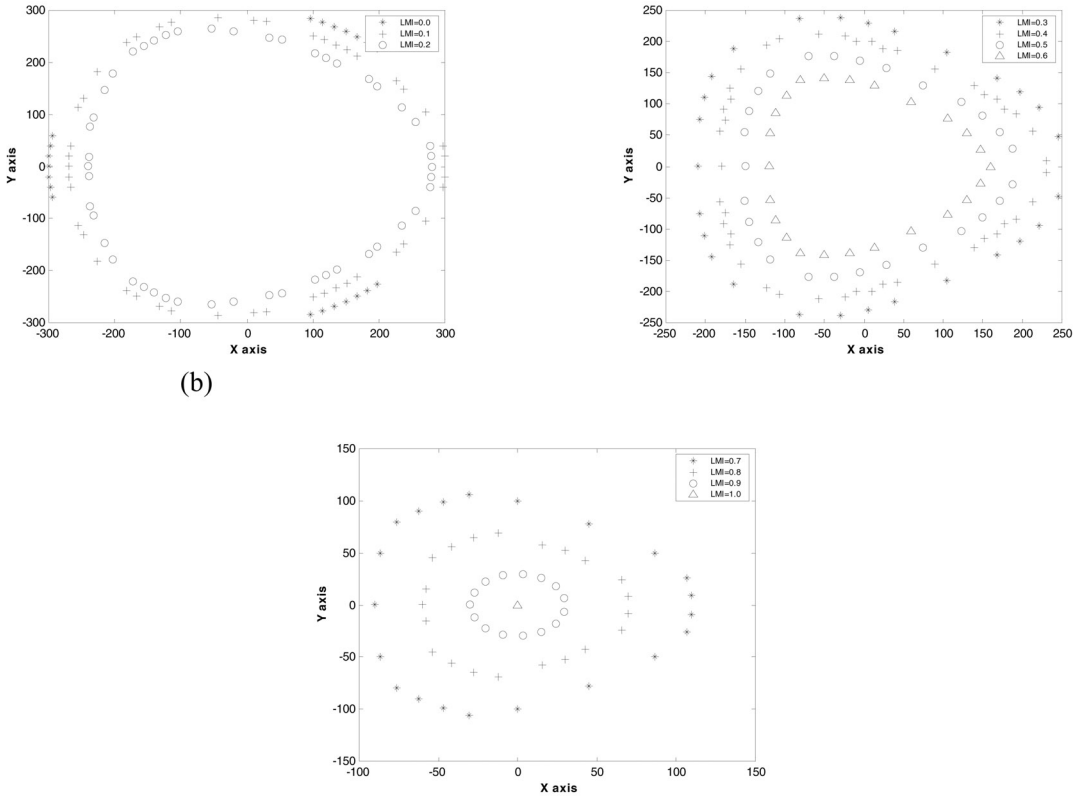

Fig. 16 LMI plots at $z = 550$ mm

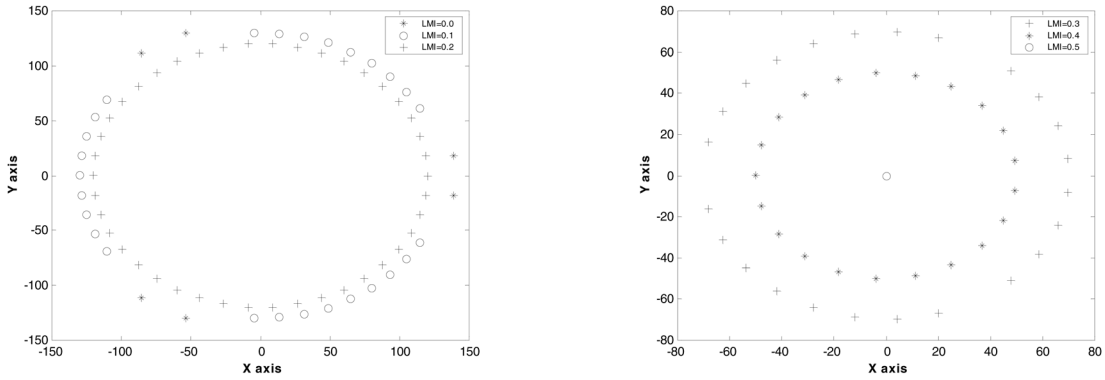

(b)

Fig. 17 LMI plots at $z = 650$ mm

Figures 15 to 17 show the LMI plots in $x-y$ planes at $z = 450$, 550 and 650 mm respectively. It is possible to determine the ratio of the maximum and minimum joint torque vector norms at some point from the LMI value. The condition when the LMI value is low indicates that the joint torque vector norm is large in some direction and exceeds the load of the actuator: i.e. a singularity is about to occur. When the LMI value is high, this means that the joint torque vector norm is uniform in all directions. However, when the eigen-ellipse converges to a line, this implies that the joint torque vector norm approaches infinity in some direction and a degree of freedom is lost. The smaller the area of the force eigen-ellipse, the farther the mechanism is from singularity. It is worth noting that the LMI value in the central region is high: i.e. the mechanism has a higher uniformity. However, the LMI values in the region away from the centre is low which means that the joint torque vector norm approaches infinity in a particular direction, the allowable load is exceeded and the mechanism is about to lose a degree of freedom in that direction. Moreover, the workspace and high LMI region are largest when $z = 450$ and smallest when $z = 650$ (see Figs 15 and 17).

6 CONCLUSIONS

In this paper, the singularity positions of a Delta-type mechanism are determined and discussed using the properties of the Jacobian matrix and quantified using some performance indices. These performance indices are defined using the column and eigenvectors of the generalized Jacobian. The distribution, shape and size of the eigen-ellipses are analysed to predict the singular positions as well as the size of the workspace. These ellipses are also used to determine the best and worst working configurations of the parallel mechanism. This information is very useful for planning tasks, determining loading conditions and path planning for parallel-type robots.

REFERENCES

1 **Stewart, D.** A platform with six degrees of freedom. *Proc. Instn Mech. Engrs*, 1965, **180**, 371–386.
2 **Ficher, E. F.** A Stewart platform-based manipulator: general theory and practical construction. *Int. J. Robotics Res.*, 1986, **5**, 157–182.
3 **Clavel, R.** Delta, a fast robot with parallel geometry. *In Proceedings of 18th International Symposium on Industrial Robots (ISIR)*, 1988, pp. 91–100.
4 **Gosselin, C.** and **Angeles, J.** The optimum kinematic design of a planar three-degree-of-freedom parallel manipulator. *Trans. ASME, J. Mech. Des.*, 1988, **110**, 35–41.
5 **Gosselin, C. M.** Parallel computational algorithms for the kinematics and dynamics of planar and spatial parallel manipulators. *Trans. ASME, J. Dynamic Syst. Measmt and Control*, 1996, **118**, 22–28.
6 **Zanganeh, K. E.** and **Sinatra, R.** Kinematics and dynamics of a six-degree-of-freedom parallel manipulator with revolute legs. *Robotica*, 1997, **15**, 385–394.
7 **Wang, J.** and **Gosselin, C. M.** Kinematic analysis and singularity representation of spatial five-degree-of-freedom parallel mechanisms. *J. Robotic Syst.*, 1997, **14**, 851–869.
8 **Gosselin, C.** Determination of the workspace of 6-DOF parallel manipulators. *Trans. ASME, J. Mech. Des.*, 1990, **112**, 331–336.
9 **Cheng, C. H.** The design and development of the Tatung TTUP3D-I parallel robot. Master's thesis, Tatung University, Taiwan, 1999.
10 **Tsai, L. W.** *Robot Analysis: the Mechanics of Serial and Parallel Manipulators*, 1999 (John Wiley, New York).
11 **Lee, M. Y., Erdman, A. G.** and **Gutman, Y.** Development of kinematic/kinetic performance tools in synthesis of multi-DOF mechanisms. *Trans. ASME, J. Mech. Des.*, 1993, **115**(3), 392–402.
12 **Lee, M. Y., Erdman, A. G.** and **Gutman, Y.** Applications of kinematic/kinetic performance tools in synthesis of multi-DOF mechanism. *Trans. ASME, J. Mech. Des.*, 1994, **116**, 392–402.